Chalcophile element processing beneath a continental arc stratovolcano

Cox, Daniel; Watt, Sebastian F.L.; Jenner, Frances E.; Hastie, Alan R.; Hammond, Samantha J.

DOI:
10.1016/j.epsl.2019.06.017

Highlights

- Pb, Bi, W, Tl, Sb and As are mobile during subduction and enriched in Antuco magmas
- Behaviour of Se is decoupled from other chalcophiles, degassing on eruption
- Cu and Ag show divergent trends consistent with crystalline sulfide fractionation
- Cu/Ag lower than MORB infers early, deep sulfide fractionation during magma ascent
- Crustal thickness, and hence depth of differentiation control on sulfide saturation

Chalcophile Element Processing Beneath a Continental Arc Stratovolcano

Daniel Cox[*1], Sebastian F. L. Watt[1], Frances E. Jenner[2], Alan R. Hastie[1], Samantha J. Hammond[2]

[1]School of Geography, Earth and Environmental Sciences, University of Birmingham, Edgbaston, Birmingham, B15 2TT, U.K.

[2]School of Environment, Earth and Ecosystem Sciences, Open University, Walton Hall, Milton Keynes, MK7 6AA, U.K.

[*]Corresponding author: DXC506@student.bham.ac.uk. School of Geography, Earth and Environmental Sciences, University of Birmingham, Edgbaston, Birmingham, B15 2TT, U.K.

Abstract

The chalcophile elements are important both in terms of their economic value and as potential tracers of magmatic processes at convergent margins. However, because of analytical difficulties, comprehensive datasets of chalcophile element concentrations for volcanic rocks are rare. Here, we present analyses of a near complete suite of chalcophile elements (S, Cu, Ag, Se, As, Sb, Sn, W, Mo, Pb, Bi, Tl, Zn, Ga, Co) for volcanic rock samples collected from a typical continental arc stratovolcano in southern Chile (Antuco). Enrichment in Pb, Bi, W, Tl, Sb and As relative to Parental-MORB indicates that these elements have been mobilised from the subducting slab into the sub-arc mantle wedge, in contrast to Cu and Ag. Very low Se concentrations suggest that Se, like S, was lost during co-eruptive degassing of the Antuco

magmas. Previous studies on oceanic arcs have demonstrated that as higher fO_2 subduction-related magmas ascend through the overlying lithosphere, magnetite fractionation may trigger sulfide fractionation during crystallisation. If such a process is extensive and has a sharp onset, this would result in a plummet in the Cu, Se and Ag contents of the residual melt. At Antuco, although a decrease in the $Fe_2O_{3(T)}$ and TiO_2 concentrations at ~55 wt.% SiO_2 (~3 wt.% MgO) indicates magnetite fractionation, this is not associated with a corresponding drop in Cu contents. Instead, we observe a general decrease in Cu and a decrease in Cu/Ag with increasing SiO_2 and decreasing MgO. Furthermore, Cu/Ag in the most primitive Antuco rocks are lower than the global MORB array, indicating that the melts were sulfide saturated at an early stage in their crustal evolution. Through modelling fractional crystallisation, we show that only a minor volume (0.5 – 0.6 vol.%) of fractionating sulfide is needed to produce divergent trends in Cu and Ag, as observed in the Antuco samples. Our results show that sulfide fractionation occurred from an early stage during the crustal evolution of Antuco's magmas. We infer that this was promoted by stalling in the lower crust, which for oxidised magmas at depths >20 km is within the sulfide stability field. However, elevated Dy_N/Yb_N of the Antuco magmas compared to oceanic island arc magmas provides an additional, or alternate mechanism to inducing sulfide fractionation in the lower crust prior to ascent, through initial garnet fractionation. Fractional crystallisation within this depth range meant that later magnetite fractionation had only a minor impact on the partitioning behaviour of the chalcophile elements. In contrast, arc magmas transiting thinner crust may not experience sulfide saturation until a later stage in their evolution, induced by magnetite fractionation. Our results imply that convergent margin crustal thickness, and therefore the depth range of magmatic differentiation, determines the dominant control on initial magmatic sulfide saturation and therefore the primary distribution of chalcophile elements. This implies that

secondary processes are required to explain the transport and concentration of sulfides and chalcophile elements at shallower crustal levels.

Keywords: chalcophile elements, sulfide, saturation, fractionation, continental arc, Antuco

1. Introduction

The chalcophiles (e.g., Cu, Ag, Se, Pb, Bi) are an important suite of elements both in terms of their economic value and their potential to investigate magmatic processes active at convergent margins (Jenner, 2017; Jenner et al., 2010; Noll Jr et al., 1996; Richards, 2009; Sillitoe, 2010; Wilkinson, 2013). Compared to the bulk continental crust, many of the economically important chalcophile elements are extremely enriched in porphyry Cu-Au deposits that are globally associated with convergent margins (Sillitoe, 2010; Wilkinson, 2013). Because primitive subduction-related magmas are not enriched in Cu, Ag, Se or Au relative to mid-ocean ridge basalt (MORB) magmas, there has been considerable debate regarding the crustal processes that contribute to the formation of magmatic-hydrothermal ore deposits (Chiaradia, 2014; Jenner, 2017; Jenner et al., 2010; Lee et al., 2012; Matjuschkin et al., 2016; Richards, 2009; Wilkinson, 2013). For example, although there is a global association between porphyry deposits and convergent margins (Sillitoe, 2010), the spatial distribution of these deposits is sporadic (Sillitoe, 1997) and the remainder of the bulk continental crust is notably depleted in Cu, Se and Au compared to primitive arc magmas (Jenner, 2017; Lee et al., 2012). Given that the bulk continental crust has been generated at convergent margins, these observations suggest that most arc magmas are not predisposed to fuel the formation of economically viable ore deposits (Jenner, 2017).

The way in which many chalcophile elements are processed and distributed within a magmatic system and throughout the continental crust is controlled by the stability of sulfides (Chiaradia, 2014; Lee et al., 2012; Richards, 2015). The point at which a magma becomes saturated in a sulfide phase is a function of the temperature, pressure, oxygen fugacity and composition of the magma (Matjuschkin et al., 2016; Mavrogenes and O'Neill, 1999; O'Neill and Mavrogenes, 2002; Wallace and Edmonds, 2011). Geochemical studies of volcanic glasses have demonstrated that the Cu/Ag of MORB magmas remains constant following sulfide saturation, in contrast to a decreasing post-saturation Cu/Ag in arc-related magmas (Jenner et al., 2015, 2010). These varying trends have been attributed to differences in the nature of the fractionating sulfide phase during differentiation of MORB (molten sulfide) and subduction-related (crystalline sulfide) magmas (Jenner, 2017; Jenner et al., 2010). This interpretation is supported by experimental studies indicating that Cu and Ag have similar partition coefficients with respect to molten sulfide, but that Cu is more compatible in crystalline sulfide than Ag (Li and Audétat, 2015, 2012). During differentiation of oceanic convergent margin magmas, the decrease in Cu/Ag (marking sulfide saturation and fractionation of crystalline sulfide) coincides with a sharp decrease in Fe, V, Cu, Ag, S and Au (reversing the preceding trend of increasing concentrations with increasing SiO_2 and decreasing MgO), suggesting that magnetite fractionation 'triggers' reduction-related sulfide saturation (the 'Magnetite Crisis'; Jenner et al., 2010) during the evolution of oceanic arc magmas (Chiaradia, 2014; Jenner, 2017). Although the 'Magnetite Crisis' potentially controls sulfide processing and the fate of chalcophile elements during island arc-magmatic evolution, such a mechanism has not been fully explored within a continental arc.

Despite the importance of the chalcophile elements for understanding both mantle and crustal processes, they are still a relatively under-studied suite of elements. This is partly because elements such as Se and Ag, which can be used in conjunction with Cu to place constraints

on the timing of sulfide saturation (see Jenner, 2017, and references therein), are difficult to analyse in both natural and experimental materials (Jenner and Arevalo, 2016). Thus, studies of chalcophile element processing at continental arcs have focussed mainly on whole rock Cu systematics, arguing that most arc magmas reach sulfide saturation during crustal differentiation (Chiaradia, 2014; Jenner, 2017; Lee et al., 2012; Richards, 2015). This is supported by observations of magmatic sulfide inclusions across a broad range of bulk compositions in Ecuadorian arc volcanic rocks, hosted predominantly in magnetite but also in silicate phases (Georgatou et al., 2018).

Chiaradia (2014) used Cu systematics to argue that magmas erupting through thicker crust (>30 km) are of calc-alkaline affinity and require smaller proportions of crystallisation to reach sulfide saturation compared to tholeiitic magmas erupting through thinner crust (<20 km), as a consequence of their higher H_2O and fO_2. This would thus influence the timing of magnetite-triggered sulfide fractionation and the resulting drop in total Fe content and fO_2 of the evolving magma. However, experimental constraints suggest an alternative explanation (Matjuschkin et al., 2016), showing that with increased pressure, and therefore depth, the sulfide stability field shifts to higher fO_2. In conjunction with this widening of the sulfide stability field with depth, Jenner (2017) used the Cu deficit and the significantly lower Cu/Ag of the bulk continental crust compared to mantle-derived melts to argue that continental crust formation is dominated by the addition of magmas that fractionate high Cu/Ag sulfides at the base of the continental crust (i.e. in a deep crustal hot zone; cf. Annen et al., 2006), prior to magma ascent to higher crustal levels.

Alternatively, Tang et al. (2018) argue that the Fe-depleting trend (i.e., calc-alkaline series) observed in magmas erupting through thick crust is attributable to garnet fractionation, from magmas that have initial fO_2 comparable to MORB. Furthermore, Tang et al. (2018) suggest that magmas erupting through thick continental crust inherit their high fO_2 (>MORB) as a

consequence of this garnet fractionation. However, the limited overlap between the garnet stability field and the crustal depth range of magmatic differentiation (Alonso-Perez et al., 2009) suggests that garnet fractionation is unlikely to explain the higher fO_2 of all arc magmas, particularly those erupted on thinner crust, and high fO_2 compared to MORB (Matjuschkin et al., 2016) appears to be a ubiquitous characteristic of arc magmas prior to the earliest stages of their differentiation (Richards, 2015; Kelley and Cottrell, 2012). As the solubility of S decreases with decreasing total Fe content of a magma, garnet fractionation would promote sulfide fractionation during magmatic differentiation at high pressures. Regardless of whether the 'Magnetite Crisis', a shift in the sulfide stability field with pressure (depth), garnet fractionation, or potentially a combination of the above processes are the 'trigger' for sulfide saturation, there is an emerging consensus that most continental arc volcanic rocks should fractionate sulfide in the lower crust prior to ascent. As a result, continental arc volcanic rocks should have lower Cu/Ag than primitive arc magmas and the entire oceanic crust, but there is a lack of reliable Cu/Ag in the literature to test this hypothesis.

Here, we present major and trace element volcanic rock compositions from Antuco Volcano, Chile, a typical continental arc stratovolcano, in order to characterise chalcophile behaviour during the generation and subsequent processing of magmas through a continental arc. Bulk compositions at Antuco span basaltic to andesitic compositions (Lopez-Escobar et al., 1981; Martínez et al., 2018), and are interpreted to initially stall and crystallise at the base of the continental crust (~40 km) prior to ascent and shallower crystallisation (~0.9 – 1.5 kbar [~2 – 5 km]; Martínez et al., 2018). This represents an ideal setting to test current models of chalcophile element processing within a continental arc, which are based on inferences drawn from oceanic arcs or datasets limited principally to Cu analyses. By generating a novel dataset that includes a near complete suite of chalcophile elements (S, Cu, Ag, Se, As, Sb, Sn,

W, Mo, Pb, Bi, Tl, Zn, Ga, Co), we seek to refine the understanding of the controls of chalcophile element distribution in continental arcs.

2. Tectonic setting and geology of Antuco Volcano

Volcanism in the South American Andes has been divided into four zones, the Northern, Central, Southern and Austral Volcanic zones, each of which is further divided into several segments (Stern, 2004). Antuco marks the northernmost point of the central part of the Southern Volcanic Zone (SVZ, **Fig. 1**) (Hickey-Vargas et al., 2016; Lopez-Escobar et al., 1995). Antuco is the younger (Pleistocene – Holocene age) of a pair of stratovolcanoes (the other being the Pleistocene Sierra Velluda Volcano) that form a volcanic complex at 37.2°S (Lopez-Escobar et al., 1981; Martínez et al., 2018). The Antuco – Sierra Velluda volcanic complex forms an oblique alignment (50 - 70° E of N) to the main arc (Lopez-Escobar et al., 1995). Antuco is the smaller of the two stratovolcanoes, with a basal diameter of ~11 km, rising to 2979 metres above sea level, and an estimated volume of 62 km^3 (Martínez et al., 2018).

Volcanism at Antuco has been divided into two phases – Phase 1 and Phase 2 Antuco (**Fig. 1a**) – separated by a westward directed, mid-Holocene sector collapse (Lopez-Escobar et al., 1981; Thiele et al., 1998) dated at 6.2 ka by Lohmar et al. (2005) and 4 ka by Clavero and Godoy (2010). Recently, Martínez et al. (2018) used a comprehensive dataset of ^{40}Ar / ^{39}Ar dates to further define Early (commencing at 150.4 ka) and Late (~16.3 to 6.2 ka) periods of volcanism during Phase 1. Phase 1 lavas show a slightly broader compositional range (basalt to andesite) than Phase 2 lavas (basalt to basaltic andesite) (Lohmar et al., 2005, 1999; Martínez et al., 2018).

Antuco is typical of stratovolcanoes in the SVZ, both in terms of its dimensions (Volker et al., 2011) and range of erupted compositions, but is also amongst the most isotopically

primitive volcanoes in the SVZ (Hickey-Vargas et al., 2016; Hildreth and Moorbath, 1988; Lohmar et al., 1999). Primitive rock compositions at Antuco indicate a predominantly fluid enriched, depleted-MORB mantle source, typical of the central SVZ, which has been used as an endmember to explore additional crustal-derived source enrichment further north in the SVZ (Holm et al., 2016, 2014). In a global context, the parameters defining this segment of the SVZ (Syracuse et al., 2010), including a crustal thickness of 40 km (Hickey-Vargas et al., 2016), suggest that it is a representative continental arc setting. The broad range in lava compositions and previous interpretations that the Antuco magmas stalled at the base of the continental crust prior to crystallisation at lower pressures (Martínez et al., 2018), make volcanic rocks from Antuco ideal for investigating the processing and distribution of the chalcophile elements during ascent of magmas through the continental crust.

2.1. Sample descriptions

The current study made use of twenty-six volcanic rock samples (fifteen Phase 1 and eleven Phase 2 samples), each from separate lava flows or pyroclastic units, which are thus considered to represent separate eruptive events and discrete batches of magma. The location of each sample is highlighted on the map of Antuco in **Fig. 1a**. Petrographically, all samples have a porphyritic texture. The groundmass is generally cryptocrystalline (crystals too small to identify) and varies from light grey to dark in colour. Phenocryst phases are dominated by plagioclase (most common) and olivine, usually comprising *c.* 10 – 20 vol.% (all phenocrysts) of thin sections (minus vesicles; can be as great as *c.* 40 vol.% and as low as <<5 vol.%). Opaques and clinopyroxene phenocrysts are rare. Plagioclase phenocrysts are mostly subhedral to euhedral laths, and commonly display simple and albite twinning and oscillatory zoning. Coarse and fine sieve textured plagioclases are common across the samples. Olivine phenocrysts are usually anhedral (mostly rounded) and fractured. Glomerocrysts are observed in all sections and comprise plagioclase and/or olivine. Sample

195 A28-6 shows extensive Fe-oxyhydroxide alteration in both phenocryst phases and
196 groundmass. Brief sample descriptions are provided as Supplementary Data (**Appendix A**).

197 **3. Analytical Methods**

198 The major and trace element compositions of the Antuco samples were determined using
199 whole rock analysis. Weathered material was removed from the samples via hammering. To
200 avoid metal contamination, samples were crushed using a fly press and powdered in an agate
201 planetary ball mill. Samples were analysed for major elements using either X-ray
202 Fluorescence (XRF) at The School of Ocean and Earth Science, National Oceanography
203 Centre, University of Southampton, U.K., or inductively coupled plasma optical emission
204 spectrometry (ICP-OES) at The School of Earth and Ocean Sciences, Cardiff University,
205 Wales, U.K. Replicate XRF analyses were undertaken at The School of Geosciences,
206 University of Edinburgh, Scotland, U.K. to test analytical precision. The loss on ignition
207 (LOI) of each sample was measured using ~1.5 ± 0.0001 g of sample powder, baked at
208 900°C. Acid digestion of sample powders was undertaken at The Open University. 100 mg of
209 each sample powder was digested in a multi-stage HF-HNO_3 digestion process, with dry
210 down temperatures set at 65°C to minimise volatile element loss. Solutions were made up to
211 1000-fold dilutions of the original powder weight in a 2% HNO_3 solution, prior to analysis.
212 Blanks and International Standard Reference Materials were prepared in the same manner.
213 Trace elements (except Tm) were analysed using an Agilent 8800 Triple Quadrupole
214 inductively coupled plasma mass spectrometer (ICP-MS/MS; also referred to as ICP-QQQ) at
215 The School of Environment, Earth and Ecosystem Sciences, The Open University, U.K.
216 Lithium, Sc, Co, Ni, Rb, Sr, Y, Zr, Nb, Mo, Sn, Sb, Cs, Ta, W, Tl, Th and U were analysed in
217 a no gas mode, the REE, S, As, Ba, Hf and Se were analysed in reactive O_2 gas mode, and V,
218 Cr, Cu, Zn, Ga, Ge, Pb and Bi were analysed in collisional He gas mode. Ag was analysed in
219 reactive NH_3 gas mode, and an offline correction to remove ZrO interferences was

subsequently employed. An online standard (containing Be, Rh, In and Tm) was run at the same time as samples and unknowns and used to monitor and correct for drift. Thulium was obtained through ICP-MS analysis at Cardiff University. Data accuracy was assessed using the International Standard Reference Materials JB1a, JA2, JG1a, BHVO-2 and DNC-1. Analyses of International Standard Reference Materials fall mostly within 5 % of published values for all major and trace elements. Exceptions include Se (10 %), Pb (11 %), As (50 %), W (30%) and Ge (7 %); however, the relative standard deviations of repeat analyses for these elements are mostly ≤7 %. We still report values for all these elements, given that International Standard Reference Material values for the chalcophile elements as a whole are not as well constrained as other trace elements (Jenner and Arevalo, 2016), with some chalcophile elements undetermined in some standards [for example, those for As in BHVO-2 are only constrained using a single analytical technique (Jochum et al., 2016)]. No suitable published values for Ag for the reference matierals we used were available, and therefore we defined values used in our calibraion line using standard addition methods. Complete analyses, including International Standard Reference Materials are provided as Supplementary Data (**Appendix B**, **Tables B1** and **B2**).

4. Geochemical Results

In terms of classification, both Phase 1 and Phase 2 samples span a similar range on a total alkali against silica (TAS) plot (**Fig. 2a**). Phase 1 samples range from basalt to andesite, with Phase 2 samples ranging from basaltic-andesite to andesite; however, two samples, one from each phase, classify as trachy-andesite. The majority of samples plot in the calc-alkaline field on an AFM (alkali – FeO – MgO) ternary plot (**Fig. 2b**) following the boundaries of Kuno (1968) and Irvine and Baragar (1971).

Antuco samples range from 51.6 to 62.3 wt.% SiO_2 and 1.5 to 6.7 wt.% MgO (anhydrous values) (**Fig. 3** and **Appendix C**, **Figs. C1** and **C2**). Titanium dioxide, Fe_2O_3 (as total Fe) and V display broadly similar trends, all increasing with increasing SiO_2, reaching a maximum of 1.6 wt.%, 10.9 wt.% and ~290 ppm, respectively at ~54-55 wt.% SiO_2, before decreasing with further increasing SiO_2 (**Fig. 3**). The trends in V, TiO_2 and Fe_2O_3 are also seen when plotted against MgO, reaching a maximum at ~3 wt.% MgO (**Fig. C1**). Many of the Phase 2 samples have higher TiO_2 and Fe_2O_3 at a given SiO_2 (and MgO) compared to Phase 1 samples. Calcium oxide shows a positive correlation with MgO; Al_2O_3 shows a peak in contents between 3 – 4 wt.% MgO; and K_2O, Na_2O and P_2O_5 show negative correlations (**Fig. C2**). Manganese oxide shows no correlation with MgO (**Fig. C2**). Our data are consistent with the major element data discussed in detail by Martínez et al. (2018), in the most recent study of Antuco (**Figs. 2**, **3**, **C1** and **C2**).

Most of the chalcophile elements (excluding Cu and Se) show negative correlations with MgO across the Antuco sample set (**Fig. C3** and **C4**). Phase 1 samples show a broad overall decrease in Cu with increasing SiO_2 (and decreasing MgO), which follows the trend defined by sulfide saturated lava samples from Ecuador (Georgatou et al., 2018) (**Figs. 4a** and **C3a**). Additionally, Phase 1 samples show a decrease in Cu/Ag with increasing SiO_2 and decreasing MgO (**Figs. 4e** and **C3c**). Three of the ~59 – 62 wt.% SiO_2 (~1.5 – 2.5 wt.% MgO) Phase 1 samples have considerably lower Cu contents (5.4 – 25.0 ppm) and Cu/Ag (124 – 691) compared to other samples with a comparable SiO_2 and MgO (48.6 – 58.9 ppm Cu and 771 – 1497 Cu/Ag). The Cu contents of Phase 2 samples remain approximately constant with increasing SiO_2 and decreasing MgO (**Figs. 4a** and **C3a**).

At a given MgO, the most primitive (highest MgO) Antuco samples have higher Pb, Tl, Sb, As and similar Bi and W compared to the MORB array (**Fig. C4**). The contents of Mo, Sn, Cu and Ag of the most primitive Antuco samples are comparable to MORB (**Figs. C3** and

C4). The S and Se contents of the Antuco samples are considerably lower than the MORB array (**Fig. 4b** and **d**). On a Parental-MORB normalised plot (**Fig. 5a**), the Antuco samples display negative Nb-Ta anomalies (barring one showing only a negative Nb anomaly) compared to neighbouring elements. Samples also show substantial peaks (15 – 100 times Parental-MORB) in W, Tl, As, Pb, Sb and Bi relative to the REE.

5. Discussion

5.1. Subduction mobile chalcophile elements

In order to distinguish which of the chalcophile elements are mobile during subduction, Jenner (2017) normalised samples to Parental-MORB (calculated), which represents an undifferentiated melt composition, approximating that of the bulk oceanic crust, and can therefore be used to constrain the relative differences in elemental fluxes at convergent margins compared to at MOR. On a Parental-MORB normalised plot (**Fig. 5a**), the Antuco samples display geochemical signatures typical of a volcano situated above a subduction zone (e.g., Pearce et al., 2005); enrichments in mobile large ion lithophile elements (LILE) compared to the moderately mobile REE, and enrichments of the moderately mobile REE compared to the high field strength elements (HFSE). All Antuco samples display enrichments in chalcophile elements W, Tl, As, Pb, Sb and Bi (**Fig. 5a**) compared to the REE and the HFSE, demonstrating that W, Tl, As, Pb, Sb and Bi are mobile during subduction. By comparison, other chalcophile elements (Mo, Sn, Zn, Ga, Co) appear to be immobile during subduction. These findings are in general agreement with previous geochemical studies regarding the relative mobility of chalcophile elements during the petrogenesis of convergent margin magmas (Jenner, 2017; Noll Jr et al., 1996). Parental-MORB-like Cu and Ag contents of the most primitive Antuco samples indicate that neither Cu nor Ag were mobilised in a slab flux to the mantle wedge during subduction, and were thus sourced from the mantle

wedge. The minor difference in enrichment of Ag relative to Cu (**Fig. 5a**) is likely a result of early sulfide fractionation from the Antuco magmas, preferentially removing Cu (over Ag).

When plotted in isolation, the mobile (i.e., Rb, Th, Ba, U, W, Tl, As, Pb, Sb and Bi, **Fig. 5b**), moderately mobile (i.e., REE, **Fig. 5c**) and immobile (i.e., HFSE, Mo, Sn Zn, Ga, Sc and Co, **Fig. 5d**) elements show relatively smooth patterns. Additionally, each group of elements shows a slight increase in Parental-MORB normalised values with increasing incompatibility of the element during differentiation of the oceanic crust. Detailed work on the partitioning of chalcophile and siderophile elements during the differentiation of mantle-derived melts (MORB and subduction-related volcanic rocks) conducted by Jenner (2017) has shown that the majority of chalcophile and siderophile elements are incompatible during differentiation (e.g., As, Sb, Tl, Pb, W, Bi). As such, these elements are preferentially enriched in the upper oceanic crust (e.g., Evolved-MORB [at ~7 wt.% MgO]) compared to the bulk (Parental-MORB) and lower oceanic crust, and are therefore more likely to be fluxed into the sub-arc mantle wedge during arc magma genesis, relative to Cu and Ag, which are compatible and reside in the lower oceanic crust (Jenner, 2017). Hence, the slight increase in the magnitude of the enrichments of the mobile elements in the Antuco samples, which mimics the upper oceanic crustal distributions of elements, suggests that the mobile elements have been added from the subducting slab to the mantle wedge source of the Antuco magmas in roughly the same proportions as their distributions in the upper oceanic crust.

5.2. Degassing of S and Se

Sulfur is commonly degassed from magmatic systems during magma ascent and/or during subaerial eruption, and consequently, determining the pre-degassing S content of magmas is challenging (Jenner et al., 2010; Wallace and Edmonds, 2011). Previous studies have demonstrated the use of Se, Cu and Ag for reconstructing the pre-eruptive S contents (i.e.,

melt inclusion contents of S) of magmatic systems (Jenner et al., 2015, 2010). For example, during differentiation of backarc basin magmas from the Eastern Manus Basin, the initial increase in FeO, Cu, Ag and Se, but constant Cu/Ag with increasing SiO_2 (and decreasing MgO), followed by a sudden drop in Cu, Ag, Se and Cu/Ag at ~60 wt.% SiO_2 (**Fig. 4**), has been attributed to magnetite-triggered sulfide fractionation rather than Cu, Se and Ag degassing (Jenner et al., 2015, 2012, 2010). As S is an essential ingredient required for fractionation of sulfides, and also because melt inclusions from the same suite have sufficient S for the melts to be considered sulfide saturated, S degassing of the Eastern Manus Basin and other backarc basin magmas is considered to take place during eruption rather than differentiation (Jenner et al., 2015, 2010). Evidence for sulfide fractionation prior to S degassing has also been demonstrated by the presence of magmatic sulfides in convergent margin magmas (Georgatou et al., 2018; Zelenski et al., 2018), such as those from Ecuador, which show a similar range in Cu versus SiO_2 systematics to the Antuco samples (**Fig. 4a**). However, the behaviour of Cu, Ag and Se in the Manus Basin was investigated using glass samples erupted beneath a significant (>1600 m) water column. Thus, it is important to re-assess the behaviour of the chalcophile elements during subaerial eruptions.

Unlike Cu, Ag, Pb, Tl, Sb, Bi, W, Sn and As, which have contents that are comparable to or higher than MORB at Antuco, the behaviour of Se appears to be decoupled from the rest of the chalcophile elements, except S. The very low S and Se concentrations – considerably lower than Parental-MORB (**Fig. 5a**), the MORB array (**Fig. 4**) and Eastern Manus Backarc Basin samples (**Fig. 4b, d** and **C3d**) – suggests that both S and Se were degassed from the melts, during either differentiation and/or eruption. Observations of Se enrichment in volcanic plumes at Mt Etna (Floor and Román-Ross, 2012) support this interpretation. The S/Se of the Antuco samples are similar to those observed in the Eastern Manus Backarc basin suite, but are considerably lower than MORB (**Fig. 4f**), indicating that S was more volatile

than Se during degassing. Interestingly, the three samples that have the highest S/Se (i.e., the least degassed samples, approaching MORB values) have the lowest Cu contents and Cu/Ag, suggesting that sulfur degassing cannot explain the trend to low Cu with increasing evolution of the Antuco samples. Given that sulfide fractionation requires the presence of S in the melt, we consider that the degassing of S (and Se) must have predominantly taken place during eruption rather than during differentiation.

5.3. Crustal processing of the chalcophile elements

Many of the chalcophile elements either have such low sulfide-silicate melt partition coefficients ($D^{sulf\text{-}sil}$) that they cannot be used to assess whether a melt has fractionated sulfide (e.g., As, Tl, Sb, Mo, Pb, Bi), and/or they show 'mixed affinities' (e.g., In, Ga, Sn, Zn, Cd), because their bulk partitioning is controlled by a combination of silicate, oxide and sulfide minerals (Jenner, 2017). Only a few of the chalcophile elements (e.g., Cu, Ag, Se, Au) are sufficiently compatible in sulfide phases to be of use for demonstrating sulfide fractionation from an evolving melt. For example, unlike the incompatible elements (e.g., As, Pb, Sb and Tl) which show a steep increase in contents with decreasing MgO (**Fig. C4**), the contents of Cu and Ag of the Antuco samples remain approximately constant and/or show a subtle decrease with increasing SiO_2 and decreasing MgO (**Figs. 4** and **C3**). Thus, like lava samples from Ecuador (Georgatou et al., 2018), the full compositional range of Antuco's magmas have been affected by sulfide fractionation. Given the potentially limited depth range of sulfide stability in the lower crust (Matjuschkin et al., 2016), this suggests that much of the compositional diversity of these magmas was acquired at lower crustal levels (consistent with "hot zone" models; e.g., Annen et al., 2006).

Unlike samples from the Eastern Manus Backarc Basin, neither the Antuco nor the Ecuador samples show an initial increase in Cu with increasing SiO_2 (or decreasing MgO) prior to

magnetite fractionation. Broad inflections at Antuco in the trends between TiO_2, Fe_2O_3 and V with SiO_2 and MgO indicate the onset of magnetite fractionation in these magmas at ~55 wt.% SiO_2 (~3 wt.% MgO) (**Figs. 3** and **C1**). However, this does not correspond with a drop in Cu contents for any Phase 2 samples or for the majority of Phase 1 samples (**Figs. 4a** and **C3a**). A similar pattern is observed in Cu data presented by Martínez et al. (2018); some, but not all Early/Late Antuco samples (Phase 1 Antuco) display a drop in Cu contents post-55 wt.% SiO_2 (or post-3 wt.% MgO), but this drop is not observed in the post-collapse samples (Phase 2 Antuco). These systematics suggest that magnetite fractionation did not play a strong control on Cu partitioning in the Antuco magmas, because the melts were already sulfide saturated before magnetite saturation. A minor impact of magnetite fractionation on the proportion of sulfide fractionation is, however, suggested by the scatter to lower Cu/Ag of some of the Phase 1 samples at ~55 wt.% SiO_2 and ~3 wt.% MgO (**Figs. 4e** and **C3c**).

The indistinguishable Cu/Ag of MORB, oceanic island basalts, oceanic plateau basalts, primitive convergent margin magmas and mantle xenoliths has been attributed to the presence of sulfide melt in the mantle source region at each tectonic setting (Jenner, 2017; Jenner et al., 2015, 2012, 2010; Wang et al., 2018). With the exception of one sample with a Cu/Ag of 5416, the Cu/Ag of the Antuco samples are all lower than the global MORB array (**Figs. 4e** and **C3c**), even in the most primitive Antuco magmas. This may indicate that minor amounts of Cu were removed from the parental Antuco melts at an early stage in their evolution. Cu/Ag patterns across the full Antuco sample set suggest fractionation of Cu from Ag throughout the crustal differentiation of these magmas, which is consistent with crystalline, rather than a sulfide melt, fractionation (Jenner et al., 2010; Li and Audétat, 2012). Some of the most evolved Antuco samples (lowest MgO) have Cu/Ag approaching that of the bulk-continental crust (**Figs. 4e** and **C3c**). It is unlikely that an early fractionating phase, such as olivine, could cause such a drop in Cu/Ag from mantle values, given the

incompatibility of Cu and Ag in potential fractionating silicate phases (Jenner, 2017; Lee et al., 2012). We therefore suggest that sulfide fractionation began in the lower crust and at a very early stage in the evolution of Antuco's parental magmas, prior to ascent and low-pressure fractional crystallisation (**Fig. 6**). This is consistent with initial stalling and crystallisation at the base of the continental crust prior to ascent to higher crustal levels (e.g., Annen et al., 2006). Lower crustal sulfide saturation is likely a result of the increased stability of crystalline sulfides at depth (Matjuschkin et al., 2016) (**Fig. 6b**). Fractionation of crystalline sulfide at the base of the continental crust (cf. Jenner, 2017) contrasts with observations in thinner, oceanic island arc/backarc settings, where Cu and Ag systematics suggest that mantle-derived melts are sulfide undersaturated until the point of magnetite fractionation, and only fractionate sulfide after this point in their evolution (e.g., Eastern Manus Basin; Chiaradia, 2014; Jenner et al., 2012, 2010) (**Fig. 6**).

Consequently, for oxidised parental arc magmas (e.g., fO_2 of ~NNO +2; Matjuschkin et al., 2016; cf. Kelley and Cottrell, 2012; Richards, 2015), sulfides would likely be stable during stalling and subsequent differentiation in 'deep crustal hot zones' (Annen et al., 2006) where the crust is ≥ ~20 km (i.e., mid- to lower continental crust) (**Fig. 6b**). In contrast, on stalling at shallower crustal levels (i.e., <20 km), approximating that of the lower crust of oceanic island arcs, oxidised magmas would not be within the field of sulfide stability (Matjuschkin et al., 2016) (**Fig. 6b**), and would thus retain their chalcophiles until their first point of sulfide fractionation was initiated by magnetite fractionation and a fO_2-related drop in S solubility. Through this mechanism, the 'Magnetite Crisis' plays a more dominant control on the fate of the chalcophile elements in thinner, oceanic arcs than it does in arcs built on thicker crust. Crustal thickness thus exerts a fundamental control on chalcophile element distribution via its influence on initial depths of magmatic differentiation, and the stability of sulfide at these depths.

Recently, Tang et al. (2018) used an inverse correlation between $[Dy/Yb]_N$ and FeO_T/MgO of global arc magmas to argue that garnet fractionation results in the simultaneous Fe depletion and increase in fO_2 of magmas, from initial fO_2 values comparable to MORB, during early differentiation of continental arc magmas. As a consequence, because the solubility of sulfur decreases with decreasing FeO_T, if primitive magmas intruding the lower continental crust were fractionating garnet, this would be expected to induce sulfide fractionation (and would also be a mechanism to increase fO_2 of the residual magma). As such, this provides an additional mechanism for deep-crustal sulfide fractionation, distinct from pressure-related effects on the sulfide stability field (e.g., Matjuschkin et al., 2016).

A direct comparison cannot be made between our data from Antuco and the trend observed between $[Dy/Yb]_N$ and FeO_T/MgO presented by Tang et al. (2018), as the FeO_T values presented for global arc magmas are for intermediate compositions (i.e., 4 ± 1 wt.% MgO) only, highlighting garnet fractionation-induced Fe depletion. However, REE systematics presented by Davidson et al. (2013, 2007) demonstrate the difference between amphibole and garnet fractionation; amphibole fractionation will result in a decrease in Dy/Yb with increasing SiO_2, whereas garnet fractionation will result in an increase in Dy/Yb with increasing SiO_2. Thus, the decrease in Dy_N/Yb_N with increasing SiO_2, and positive correlation between Dy/Dy* and Dy_N/Yb_N of the Antuco suite is consistent with amphibole, not garnet fractionation (**Fig. 7**). The absence of amphibole phenocrysts in the Antuco samples further supports Davidson et al.'s (2007) interpretation that these REE ratios imply "cryptic amphibole fractionation".

Despite arguing that at Antuco the magmas have been affected by amphibole, rather than garnet fractionation, we do not discount Tang et al.'s (2018) suggestion that the crystallising assemblage from arc magmas is likely to transition from magnetite to garnet fractionation if the crust becomes sufficiently thick. Indeed, the noticeably higher Dy_N/Yb_N of the most

primitive Antuco samples compared to the Eastern Manus Backarc Basin suite is consistent with the fractionation of garnet (**Fig. 7**). Thus, the high Dy_N/Yb_N and low Cu/Ag of the Antuco suite could indicate that garnet and sulfide were fractionated from the most primitive Antuco magmas (during the earliest or deepest stages of magmatic differentiation), prior to ascent. Additionally, a minor initial decrease in Fe_2O_3 with increasing SiO_2 (**Fig. 3b**) supports an initial stage of garnet fractionation.

However, the degree of garnet fractionation from the Antuco magmas appears minimal (based on the Dy_N/Yb_N trends supporting a predominance of amphibole fractionation). As such, we still call upon the effect of pressure on the sulfide stability field (Matjuschkin et al., 2016) to achieve sulfide saturation in the lower continental crust and explain the overall Cu/Ag trends at Antuco, which is a satisfactory explanation especially if convergent margin magmas have a higher initial fO_2 compared to MORB or are driven to a higher fO_2 as a consequence of garnet fractionation.

To place constraints on the proportion of sulfide fractionation required to explain the Cu and Ag systematics of the Antuco magmas, we have used the following fractional crystallisation equation:

$$C_l = C_o*(F^{Do-1})$$

where, C_l is the concentration of an element in the resultant melt, C_o is the concentration of an element in the source prior to fractional crystallisation, F is the fraction of melt remaining, and D_o is the bulk-partition coefficient of an element prior to fractional crystallisation.

Starting compositions used for Cu (68.9 ppm) and Ag (0.04 ppm) are those of the most primitive (highest MgO wt.%) Antuco sample (An27-7). Partition coefficients used for Cu and Ag in crystalline (monosulfide solid solution) sulfides (Kd_{Cu}^{Sul}: 215, Kd_{Ag}^{Sul}: 24) were those derived experimentally by Li and Audétat (2012) (average of experiments LY15 and

LY17) and are chosen as they are determined under conditions that best replicated a subduction zone setting (i.e., oxidised). Available partition coefficients for Cu and Ag in plagioclase and olivine show them both to be very low at <<0.1 (Adam and Green, 2006; Ewart et al., 1973; Lee et al., 2012). As such, both plagioclase and olivine were grouped as one in the modelling calculations. For full details on the modelling parameters, see **Table 1**.

With only a minor volume (0.5 to 0.6 vol.%) of sulfide fractionation, broadly flat to slightly decreasing Cu and increasing Ag trends can be produced (**Figs. 8a** and **C5**). Consequently, as a result of the divergent trends in Cu and Ag, a continual decrease in Cu/Ag is also produced (**Fig. 8b**). These trends match those seen in Cu and Ag at Antuco and supports our conclusion that the Antuco magmas have been affected by a small degree (~0.5 vol.%) of sulfide fractionation throughout their petrogenesis.

6. Conclusion

The near complete suite of chalcophile elements were analysed in twenty-six volcanic rock samples from Antuco Volcano, Chile, which were used to investigate their processing and distribution within the magmatic system of a typical continental arc stratovolcano. Enrichments in W, Tl, As, Pb, Sb and Bi in the Antuco volcanic rocks suggest these chalcophile elements were mobilised during subduction. Additionally, the relative enrichments of these chalcophile elements indicate that the flux of elements from the oceanic crust to the mantle wedge is determined by their prior concentration in the subducting upper oceanic crust. Cu and Ag concentrations similar to the global MORB array suggest that neither Cu nor Ag were mobilised during subduction, and that Mo, Sn, Zn, Ga and Co were also immobile. Very low Se and S concentrations relative to the global MORB array reflect low-pressure degassing of these elements during eruption, preventing the reconstruction of Se systematics from subaerial volcanic rocks.

Inflections in the TiO_2, Fe_2O_3 and V concentrations, and a corresponding (minor) drop in Cu contents and Cu/Ag of some Phase 1 Antuco samples at ~55 wt.% SiO_2 and ~3 wt.% MgO, suggests that magnetite fractionation occurred during the crustal evolution of these magmas. However, in contrast to oceanic arc magmas, there is no strong correspondence between magnetite and sulfide fractionation. Mostly flat Cu and Ag trends indicate that the Antuco melts were already sulfide saturated from a very early stage in their crustal history, and well before magnetite fractionation. Fractionation of Cu from Ag (i.e., a decreasing Cu/Ag ratio throughout the evolutionary trend) suggests that the fractionating sulfide phase was crystalline and can be explained by 0.5 to 0.6% of fractionating sulfide during crustal differentiation. The low Cu/Ag of the most primitive Antuco samples compared to the global MORB array suggest an early, high-pressure stage of sulfide fractionation from the Antuco magmas. This implies that sulfide fractionation began at the base of the continental crust, in primitive magmas, and that sulfide is stable at lower crustal pressures in continental arcs, which is the predominant depth range of magmatic differentiation. As such, sulfide fractionation was not strongly influenced by magnetite fractionation, as is more likely the case in thinner, oceanic arcs. In oceanic arcs, the initial depth range of magmatic differentiation may be outside the field of sulfide stability, and magnetite thus acts as a dominant control on sulfide fractionation. We have shown that crustal thickness plays an important role in controlling the differentiation of continental arc magmas and the resulting distribution of the chalcophile elements in the arc crust. Beneath continental arcs, these processes would lead to the formation of a theoretical chalcophile-rich reservoir at or near the base of the continental crust that could be tapped to fuel ore deposit formation.

Acknowledgements

DC, SW and FJ acknowledge funding for this work, completed as part of the first author's Ph. D., from the Natural Environment Research Council (NERC) project NE/M000427/1 (Mantle volatiles: processes, reservoirs and fluxes). Frances Jenner also acknowledges funding from the NERC 'SoS Tellurium and Selenium Cycling and Supply (TeASe)' consortium grant (NE/M010848/1) and the NERC 'From Arc Magmas to Ore Systems' (FAMOS) consortium grant (NE/P017045/1). We thank Iain McDonald for support with major element analyses. Alastair Hodgetts and David Cavell are thanked for comments on earlier versions of the manuscript. Frederic Moynier (Editor), Massimo Chiaradia and an anonymous reviewer are thanked for their constructive and insightful comments during review, improving the manuscript greatly.

References

Adam, J., Green, T., 2006. Trace element partitioning between mica- and amphibole-bearing garnet lherzolite and hydrous basanitic melt: 1. Experimental results and the investigation of controls on partitioning behaviour. Contrib. to Mineral. Petrol. 152, 1–17.

Alonso-Perez, R., Müntener, O., Ulmer, P., 2009. Igneous garnet and amphibole fractionation in the roots of island arcs. Contrib. to Mineral. Petrol. 157, 541-558.

Annen, C., Blundy, J.D., Sparks, R.S.. J., 2006. The genesis of intermediate and silicic magmas in deep crustal hot zones. J. Petrol. 47, 505–539.

Chiaradia, M., 2014. Copper enrichment in arc magmas controlled by overriding plate thickness. Nat. Geosci. 7, 43–46.

Clavero, J., Godoy, E., 2010. The Late Holocene Collapse of Antuco Volcano: a Valley

535 Confined Debris Avalanche Flow, Southern Andes, Chile, in: Cities on Volcanoes 6
536 Abstracts Volume. p. 42.

537 Davidson, J., Turner, S., Handley, H., Macpherson, C., Dosseto, A., 2007. Amphibole
538 "sponge" in arc crust? Geology 35, 787-790.

539 Davdison, J., Turner, S., Plank, T., 2013. Dy/Dy*: Variations arising from mantle sources
540 and petrogenetic processes. J. Petrol. 54, 525-537.

541 Ewart, A., Bryan, W.B., Gill, J.B., 1973. Mineralogy and geochemistry of the Youger
542 Volcanic Islands of Tonga, S.W. Pacific. J. Petrol. 14, 429–465.

543 Floor, G.H., Román-Ross, G., 2012. Selenium in volcanic environments: A review. Appl.
544 Geochemistry 27, 517–531.

545 Georgatou, A., Chiaradia, M., Rezeau, H., Wälle, M., 2018. Magmatic sulphides in
546 Quaternary Ecuadorian arc magmas. Lithos 296–299, 580–599.

547 Hickey-Vargas, R., Holbik, S., Tormey, D., Frey, F.A., Moreno Roa, H., 2016. Basaltic rocks
548 from the Andean Southern Volcanic Zone: Insights from the comparison of along-strike
549 and small-scale geochemical variations and their sources. Lithos 258–259, 115–132.

550 Hildreth, W., Moorbath, S., 1988. Crustal contributions to arc magmatism in the Andes of
551 Central Chile. Contrib. to Mineral. Petrol. 98, 455–489.

552 Holm, P.M., Søager, N., Alfastsen, M., Bertotto, G.W., 2016. Subduction zone mantle
553 enrichment by fluids and Zr–Hf-depleted crustal melts as indicated by backarc basalts of
554 the Southern Volcanic Zone, Argentina. Lithos 262, 135–152.

555 Holm, P.M., Søager, N., Dyhr, C.T., Nielsen, M.R., 2014. Enrichments of the mantle sources
556 beneath the Southern Volcanic Zone (Andes) by fluids and melts derived from abraded
557 upper continental crust. Contrib. to Mineral. Petrol. 167, 1–27.

558 Irvine, T.N., Baragar, W.R.A., 1971. A guide to the chemcial classification of the common
559 volcanic rocks. Can. J. Earth Sci. 8, 523–548.

560 Jenner, F.E., 2017. Cumulate causes for the low contents of sulfide-loving elements in the
561 continental crust. Nat. Geosci. 10, 524–529.

562 Jenner, F.E., Arculus, R.J., Mavrogenes, J.A., Dyriw, N.J., Nebel, O., Hauri, E.H., 2012.
563 Chalcophile element systematics in volcanic glasses from the northwestern Lau Basin.
564 Geochemistry, Geophys. Geosystems 13. https://doi.org/10.1029/2012GC004088

565 Jenner, F.E., Arevalo, R.D., 2016. Major and Trace Element Analysis of Natural and
566 Experimental Igneous Systems using LA–ICP–MS. Elements 12, 311–316.

567 Jenner, F.E., Hauri, E.H., Bullock, E.S., Konig, S., Arculus, R.J., Mavrogenes, J. a.,
568 Mikkelson, N., Goddard, C., 2015. The competing effects of sulfide saturation versus
569 degassing on the behavior of the chalcophile elements during the differentiation of
570 hydrousmelts Frances. Geochemistry Geophys. Geosystems 16, 1490–1507.

571 Jenner, F.E., O'Neill, H.S.C., 2012. Analysis of 60 elements in 616 ocean floor basaltic
572 glasses. Geochemistry, Geophys. Geosystems 13, 1–11.

573 Jenner, F.E., O'Neill, H.S.C., Arculus, R.J., Mavrogenes, J.A., 2010. The magnetite crisis in
574 the evolution of arc-related magmas and the initial concentration of Au, Ag and Cu. J.
575 Petrol. 51, 2445–2464.

576 Jochum, K.P., Weis, U., Schwager, B., Stoll, B., Wilson, S.A., Haug, G.H., Andreae, M.O.,
577 Enzweiler, J., 2016. Reference Values Following ISO Guidelines for Frequently
578 Requested Rock Reference Materials. Geostand. Geoanalytical Res. 40, 333–350.

579 Kelley, K.A., Cottrell, E., 2012. The influence of magmatic differentiation on the oxidation
580 state of Fe in a basaltic arc magma. Earth Planet. Sci. Lett. 329-330, 109-121.

581 Kuno, H., 1968. Differentiation of basalt magmas, in: Basalts: The Poldervaart Treatise on
582 Rocks of Basaltic Composition. John Wiley and Sons, New York, pp. 623–688.

583 Le Bas, M.J., Le Maitre, R.W., Streckeisen, A., Zanettin, B., 1986. A chemical classification
584 of volcanic rocks based on the total alkali-silica diagram. J. Petrol. 27, 745–750.

585 Lee, C.T.A., Luffi, P., Chin, E.J., Bouchet, R., Dasgupta, R., Morton, D.M., Le Roux, V.,
586 Yin, Q., Jin, D., 2012. Copper systematics in arc magmas and implications for crust-
587 mantle differentiation. Science 336, 64–68.

588 Li, Y., Audétat, A., 2015. Effects of temperature, silicate melt composition, and oxygen
589 fugacity on the partitioning of V, Mn, Co, Ni, Cu, Zn, As, Mo, Ag, Sn, Sb, W, Au, Pb,
590 and Bi between sulfide phases and silicate melt. Geochim. Cosmochim. Acta 162, 25–
591 45.

592 Li, Y., Audétat, A., 2012. Partitioning of V, Mn, Co, Ni, Cu, Zn, As, Mo, Ag, Sn, Sb, W, Au,
593 Pb, and Bi between sulfide phases and hydrous basanite melt at upper mantle conditions.
594 Earth Planet. Sci. Lett. 355–356, 327–340.

595 Lohmar, S., Lopez-Escobar, L., Moreno, H., 2005. Preliminary Comparison Between Antuco
596 and Sierra Velluda Volcanoes (Southern Andes).

597 Lohmar, S., Lopez-Escobar, L., Moreno, H., Deruelle, B., 1999. Antuco Volcano: One of the
598 isotopically most primitive stratovolcanoes of the Southern Andes (37 25'S), in: Fourth
599 International Symposium on Andean Geodynamics. pp. 437–440.

600 Lopez-Escobar, L., Cembrano, J., Moreno, H., 1995. Geochemistry and tectonics of the
601 Chilean southern Andes basaltic Quaternary volcanism (37-46°S). Rev. Geol. Chile 22,
602 219–234.

603 Lopez-Escobar, L., Vergara, M., Frey, F.A., 1981. Petrology and geochemistry of lavas from

604 Antuco Volcano, a basaltic volcano of the Southern Andes (37 25'S). J. Volcanol.
605 Geotherm. Res. 11, 329–352.

606 Marshall, D., 1996. Ternplot: An excel spreadsheet for ternary diagrams. Comput. Geosci.
607 22, 697–699.

608 Martínez, P., Singer, B.S., Roa, H.M., Jicha, B.R., 2018. Volcanologic and petrologic
609 evolution of Antuco-Sierra Velluda, Southern Andes, Chile. J. Volcanol. Geotherm. Res.
610 349, 392–408.

611 Matjuschkin, V., Blundy, J.D., Brooker, R.A., 2016. The effect of pressure on sulphur
612 speciation in mid- to deep-crustal arc magmas and implications for the formation of
613 porphyry copper deposits. Contrib. to Mineral. Petrol. 171, 66.
614 https://doi.org/10.1007/s00410-016-1274-4

615 Mavrogenes, J.A., O'Neill, H.S.C., 1999. The relative effects of pressure, temperature and
616 oxygen fugacity on the solubility of sulfide in mafic magmas. Geochim. Cosmochim.
617 Acta 63, 1173–1180.

618 Noll Jr, P.D., Newsom, H.E., Leeman, W.P., Ryan, J.G., 1996. The role of hydrothermal
619 fluids in teh production of subduction zone magmas: Evidence from siderophile and
620 chalcophile trace elements and boron. Geochim. Cosmochim. Actamica 60, 587–611.

621 O'Neill, H.S.C., Mavrogenes, J.A., 2002. The Sulfide Capacity and the Sulfur Content at
622 Sulfide Saturation of Silicate Melts at 1400°C and 1 bar. J. Petrol. 43, 1049–1087.

623 Pearce, J.A., Stern, R.J., Bloomer, S.H., Fryer, P., 2005. Geochemical mapping of the
624 Mariana arc-basin system: Implications for the nature and distribution of subduction
625 components. Geochemistry, Geophys. Geosystems 6, 1–27.

626 Richards, J.P., 2015. The oxidation state, and sulfur and Cu contents of arc magmas:

627 implications for metallogeny. Lithos 233, 27–45.

628 Richards, J.P., 2009. Postsubduction porphyry Cu-Au and epithermal Au deposits: Products
629 of remelting of subduction-modified lithosphere. Geology 37, 247–250.

630 Rudnick, R.L., Gao, S., 2003. Composition of the Continental Crust, in: Treatise on
631 Geochemistry: The Crust. pp. 1–64.

632 Sillitoe, R.H., 2010. Porphyry Copper Systems. Econ. Geol. 105, 3–41.

633 Sillitoe, R.H., 1997. Characteristics and controls of the largest porphyry copper- gold and
634 epithermal gold deposits in the circum- Pacific region. Aust. J. Earth Sci. 44, 373–388.

635 Stern, C.R., 2004. Active Andean volcanism: its geologic and tectonic setting. Rev. geológica
636 Chile 31, 161–206.

637 Sun, S.-S., McDonough, W.F., 1989. Chemical and isotopic systematics of oceanic basalts:
638 implications for mantle composition and processes. Geol. Soc. London Spec. Publ. 42,
639 313-345.

640 Syracuse, E.M., van Keken, P.E., Abers, G.A., 2010. The global range of subduction zone
641 thermal models. Phys. Earth Planet. Inter. 183, 73–90.

642 Tang, M., Erdman, M., Eldridge, G., Lee, C.-T.A., 2018. The redox "filter" beneath
643 magmatic orogens and the formation of continental crust. Sci. Adv. 4, 1–7.

644 Thiele, R., Moreno, H., Elgueta, S., Lahsen, A., Rebolledo, S., Petit-Breuilh, M.E., 1998.
645 Evolución geológico-geomorfológico cuaternaria del tramo superior del valle del río
646 Laja. Rev. Geológica Chile 25, 229–253.

647 Volker, D., Kutterolf, S., Wehrmann, H., 2011. Comparative mass balance of volcanic
648 edifices at the southern volcanic zone of the Andes between 33 S and 46 S. J. Volcanol.

649 Geotherm. Res. 205, 114–129.

650 Wallace, P.J., Edmonds, M., 2011. The Sulfur Budget in Magmas: Evidence from Melt
651 Inclusions, Submarine Glasses, and Volcanic Gas Emissions. Rev. Mineral.
652 Geochemistry 73, 215–246.

653 Wang, Z., Becker, H., Liu, Y., Hoffmann, E., Chen, C., Zou, Z., Li, Y., 2018. Constant
654 Cu/Ag in upper mantle and oceanic crust: Implications for the role of cumulates during
655 the formation of continental crust. Earth Planet. Sci. Lett. 493, 25–35.

656 Wilkinson, J.J., 2013. Triggers for the formation of porphyry ore deposits in magmatic arcs.
657 Nat. Geosci. 6, 917–925.

658 Zelenski, M., Kamenetsky, V.S., Mavrogenes, J.A., Gurenko, A., Danyushevsky, L. V., 2018.
659 Silicate-sulfide liquid immiscibility in modern arc basalt (Tolbachik volcano,
660 Kamchatka): Part I. Occurrence and compositions of sulfide melts. Chem. Geol. 478,
661 102–111.

662

663 **Figure Captions**

664 Figure 1: (a) Simplified geological map of Antuco Volcano, Chile. Sample locations
665 highlighted with filled circles. Geological map adapted after Martínez et al. (2018). Base
666 image from Google Earth (2018). (b) Location map of Antuco Volcano, highlighting its
667 location at the northern end of the Central Southern Volcanic Zone. The reader is referred to
668 the online version of this article for interpretation of the figure(s) in colour.

669 Figure 2: (a) Total-alkali-silica (TAS) plot of the Antuco samples. Antuco Phase 1 samples of
670 the current study range in composition from basalt to andesite, with one classifying as a
671 trachy-andesite. Antuco Phase 2 samples of the current study have a slightly narrower

672 compositional range from basaltic andesite to andesite, again with one classifying as a trachy-
673 andesite. Also plotted are samples analysed by Martínez et al. (2018) from Antuco (M18),
674 which display very similar compositional ranges to the current study. Classification fields as
675 of Le Bas et al. (1986). (b) Alkali-iron-magnesium (AFM) ternary plot of the Antuco
676 samples. The majority of both Phase 1 and 2 samples plot in the calc-alkaline field. Ternary
677 plot constructed in TernPlot (Marshall, 1996), using the boundary lines of Kuno (1968) and
678 Irvine and Baragar (1971).

679 Figure 3: Select major element (TiO_2, Fe_2O_3) and Vanadium bivariate plots (vs. SiO_2) of the
680 Antuco samples. Inflections in TiO_2, Fe_2O_3 and V at ~55 wt.% SiO_2 highlight the onset of
681 magnetite fractionation in the Antuco magmas. Also plotted are samples from Antuco
682 analysed by Martínez et al. (2018) (M18). Samples from M18 display similar concentration
683 ranges and show inflections in TiO_2, Fe_2O_3 and V.

684 Figure 4: Select trace element (Cu, Ag, Se, and S) bivariate plots (vs. SiO_2, FeO) of the
685 Antuco samples. (a) The continual decrease in Cu contents with increasing SiO_2 shown by
686 Phase 1 samples (and Early Antuco samples of M18) is similar to that seen in Cu data from
687 sulfide saturated Ecuadorian volcanoes [data from Georgatou et al., 2018 (G18)]. (a, c, d, e)
688 The trends seen in Cu at Antuco and in Ecuadorian volcanoes are different to that seen in data
689 from the Eastern Manus Backarc Basin (EMBB), where Cu (and Ag, Se) contents increase
690 with increasing SiO_2, before rapidly decreasing after the onset of magnetite fractionation at
691 ~58 wt.% SiO_2 [data from Jenner et al., 2012 (J12)]. (b, d, f) The S and Se contents of the
692 Antuco samples are considerably lower than the Global (Pacific and Atlantic) MORB array
693 [data from Jenner and O'Neill, 2012], suggesting they were both degassed from the Antuco
694 magmas. This is unlike that seen in Se data from the Eastern Manus Backarc Basin (EMBB),
695 where Se contents increase then decrease with increasing SiO_2, attributed to magnetite

696 induced sulfide fractionation [data from Jenner et al., 2012 (J12)]. Bulk continental crust
697 composition from Rudnick and Gao (2003) (RG03).

698 Figure 5: Parental-MORB normalised (values from Jenner, 2017) multi-element plots. (a)
699 Complete multi-element plot of Antuco samples compared to the bulk-continental crust [data
700 from Rudnick and Gao, 2003]. Element ordering reflects increasing incompatibility (from
701 right to left) of the elements during low-pressure differentiation of MORB (see Jenner, 2017).
702 Isolated mobile (b), moderately mobile (c) and immobile (d) Parental-MORB normalised
703 multi-element plots show that the mobile chalcophile elements are considerably more
704 enriched in the Antuco magmas compared to the REE and HFSE. Additionally, the relatively
705 unfractionated patterns displayed by the Parental-MORB normalised mobile chalcophile
706 elements, together with the slight increase in values with increasing incompatibility during
707 MORB differentiation, indicates that these elements were added into the mantle wedge in
708 roughly similar proportions as they are found in the upper oceanic crust [i.e., pattern
709 comparable to Evolved-MORB, as presented by Jenner (2017) (J17)].

710 Figure 6: (a) Schematic illustration comparing the processing of Cu beneath thick (≥30 km)
711 and thin (≤20 km) overriding crust at convergent margins. Fluid mobile chalcophile elements
712 (W, Tl, Sb, Pb, As, Bi) are added to the mantle wedge via a slab flux, whereas the immobile
713 chalcophile elements (Cu, Ag) are retained in the lower oceanic crust. Thicker overriding
714 (continental) crust promotes early sulfide fractionation from the Antuco magmas (and
715 removal of Cu from the ascending magma) due to the increased stability of sulfides at higher
716 fO_2 with increased pressure (and therefore depth) (**inset b**; adapted after Matjuschkin et al.,
717 2016). The thinner nature of the overriding crust at island arcs (IA) and backarc basins (BAB)
718 means sulfides are less likely to be stable at the base of the crust and therefore do not
719 fractionate, allowing Cu contents to increase as magmas ascends prior to magnetite induced
720 sulfide fractionation.

721 Figure 7: Rare Earth Element systematics of the Antuco magmas. Decreasing Dy_N/Yb_N with
722 increasing SiO_2 (a), and a positive correlation between Dy/Dy* and Dy_N/Yb_N (b) suggest
723 "cryptic amphibole fractionation" from the Antuco magmas (e.g., Davidson et al., 2013,
724 2007). EMBB (J12): Eastern Manus Backarc Basin (data from Jenner et al., 2012).
725 Normalising values from Sun and McDonough (1989). Grt: garnet; Amph: amphibole.

726 Figure 8: Trace element modelling of fractional crystallisation. Minimal sulfide fractionation
727 (0.5 – 0.6 vol.%) is required to produce divergent trends in Cu (a) and Ag (**Appendix C**, **Fig.**
728 **C5**) and Cu/Ag approaching that of the bulk continental crust (b), as observed in the Antuco
729 samples. Starting Cu and Ag compositions used were those of the most primitive (highest
730 MgO wt.%) Antuco sample (An27-7). The composition of the bulk continental crust is
731 plotted for comparison [data from Rudnick and Gao, 2003].

Graphical Abstract (for review)

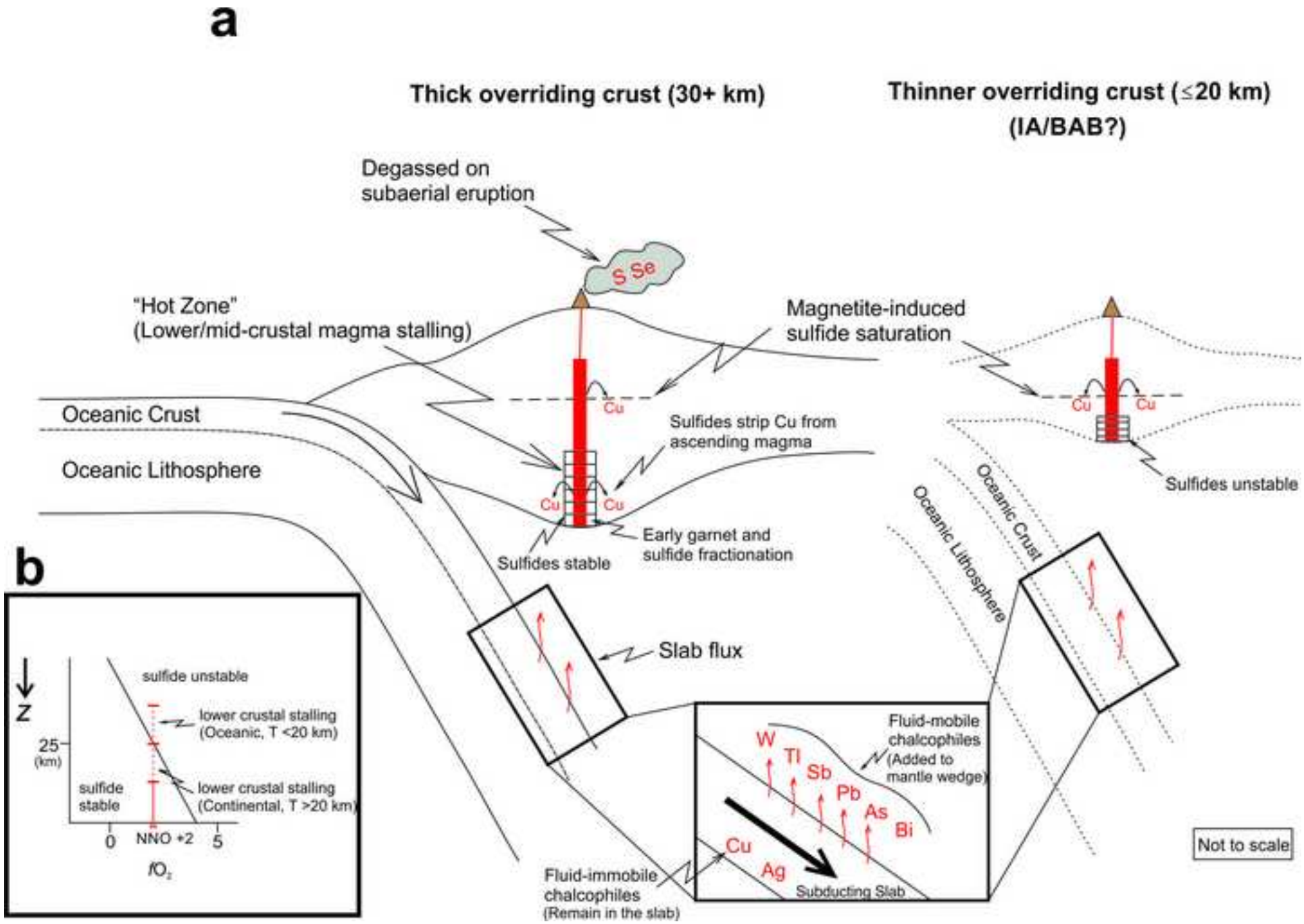

Figure

Click here to download Figure: Cox_et_al_Figure1.pdf

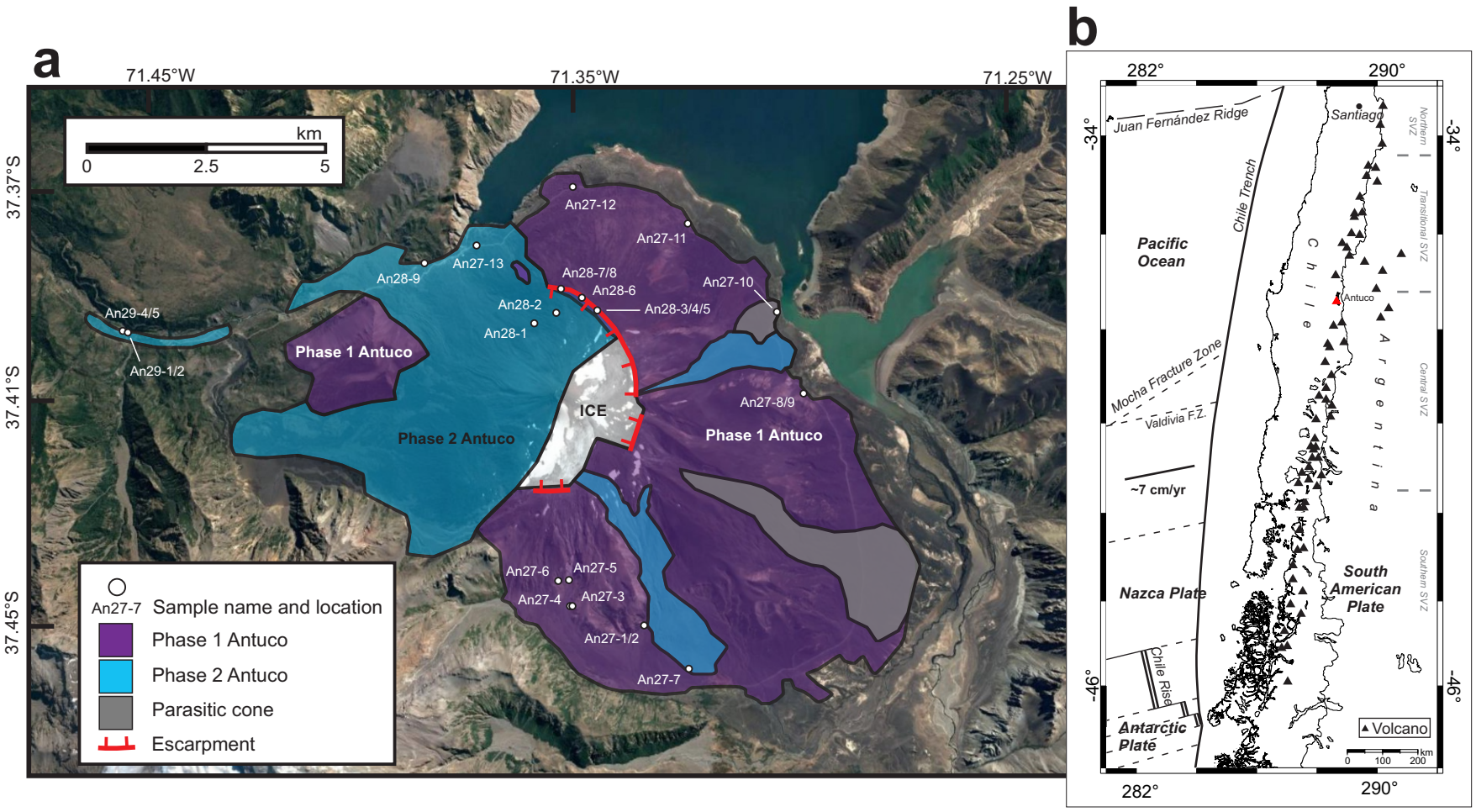

Figure

Click here to download Figure: Cox_et_al_Figure2.pdf

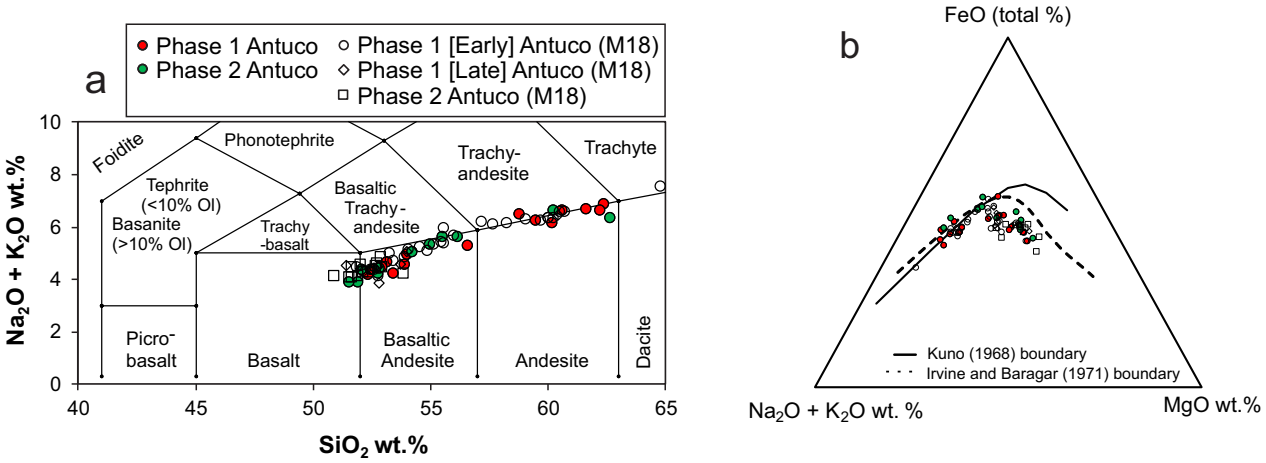

Figure

Click here to download Figure: Cox_et_al_Figure3.pdf

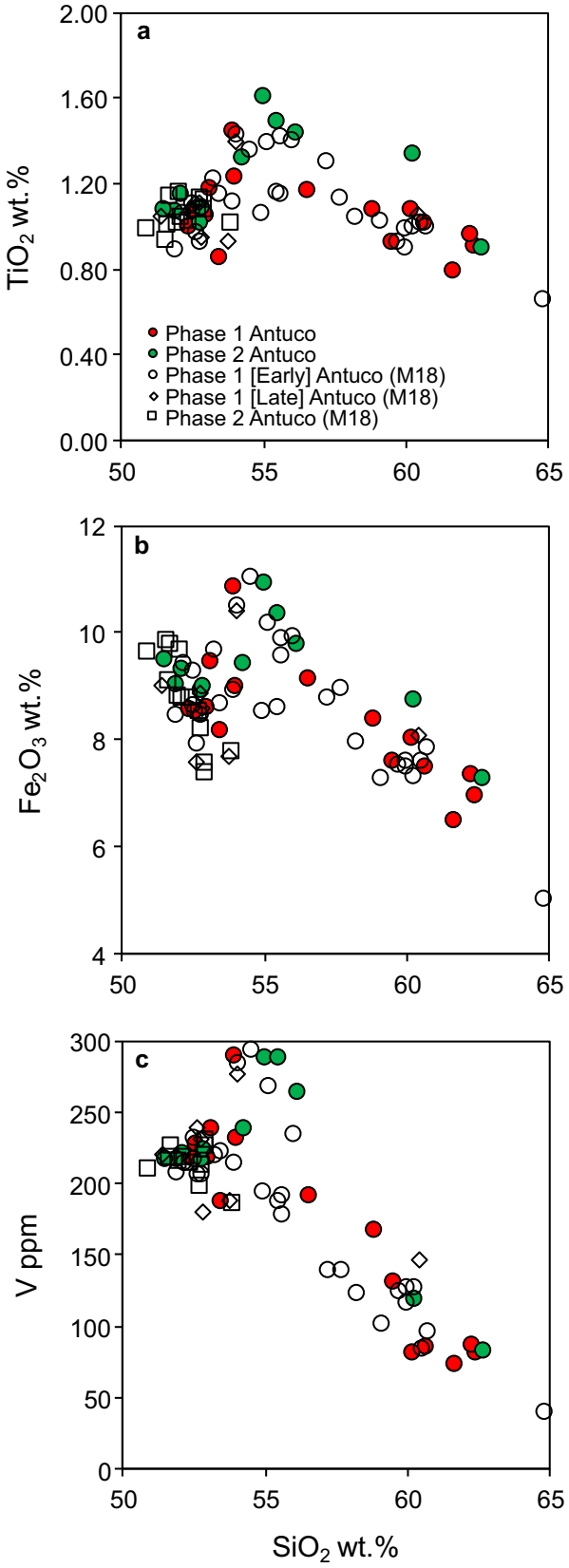

Figure

Click here to download Figure: Cox_et_al_Figure4.pdf

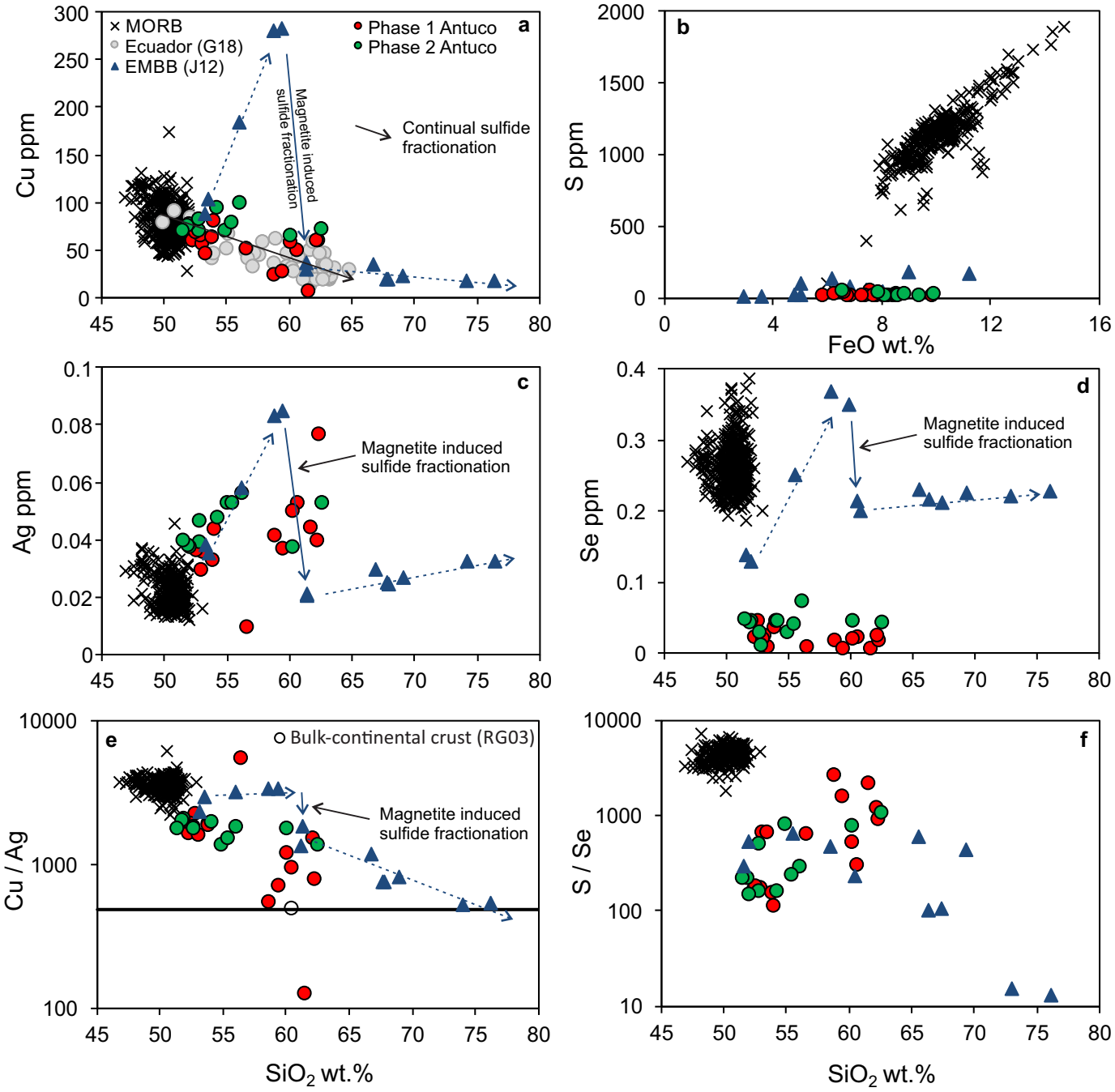

Figure

Click here to download Figure: Cox_et_al_Figure5.pdf

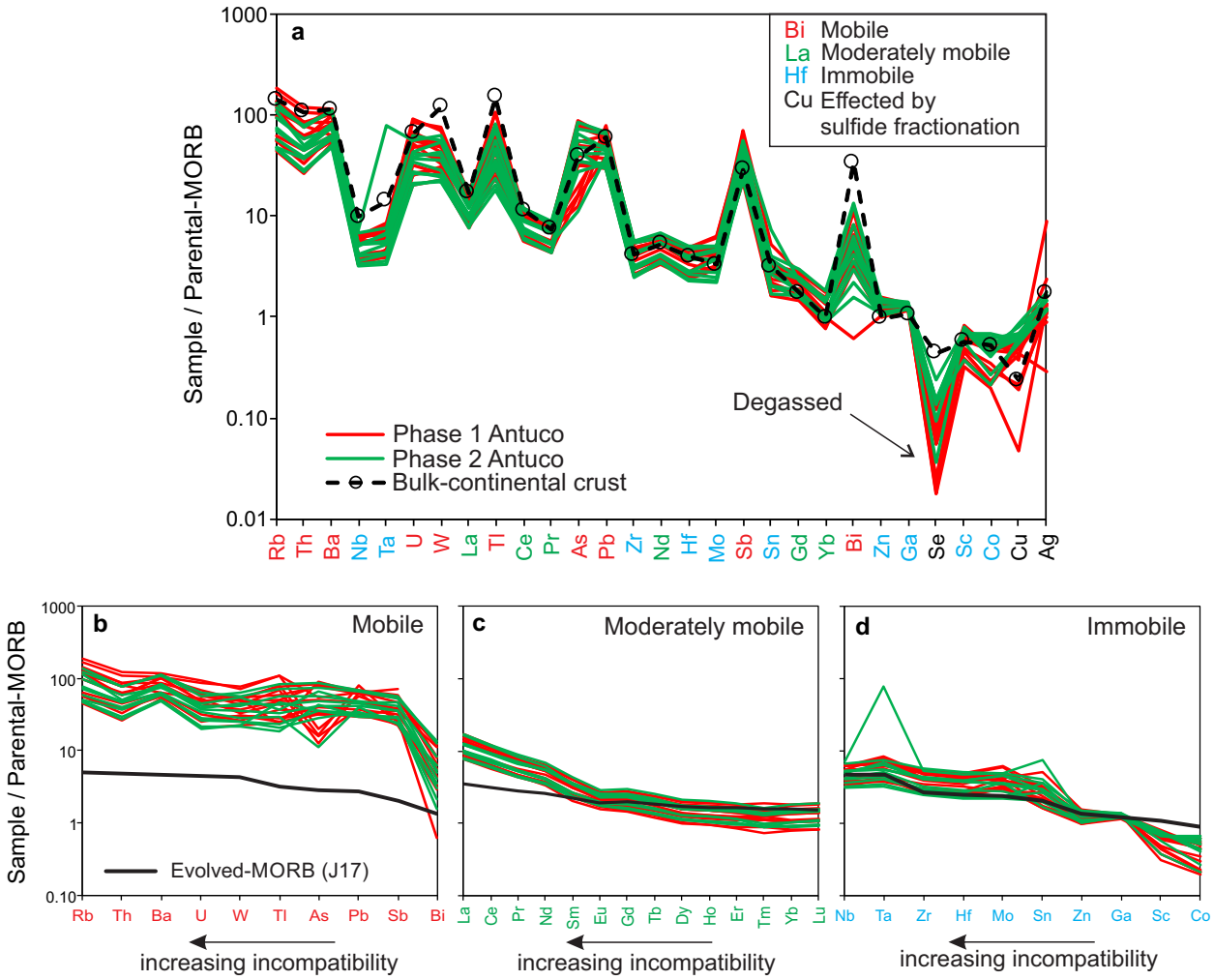

Figure

Click here to download Figure: Cox_et_al_Figure6.pdf

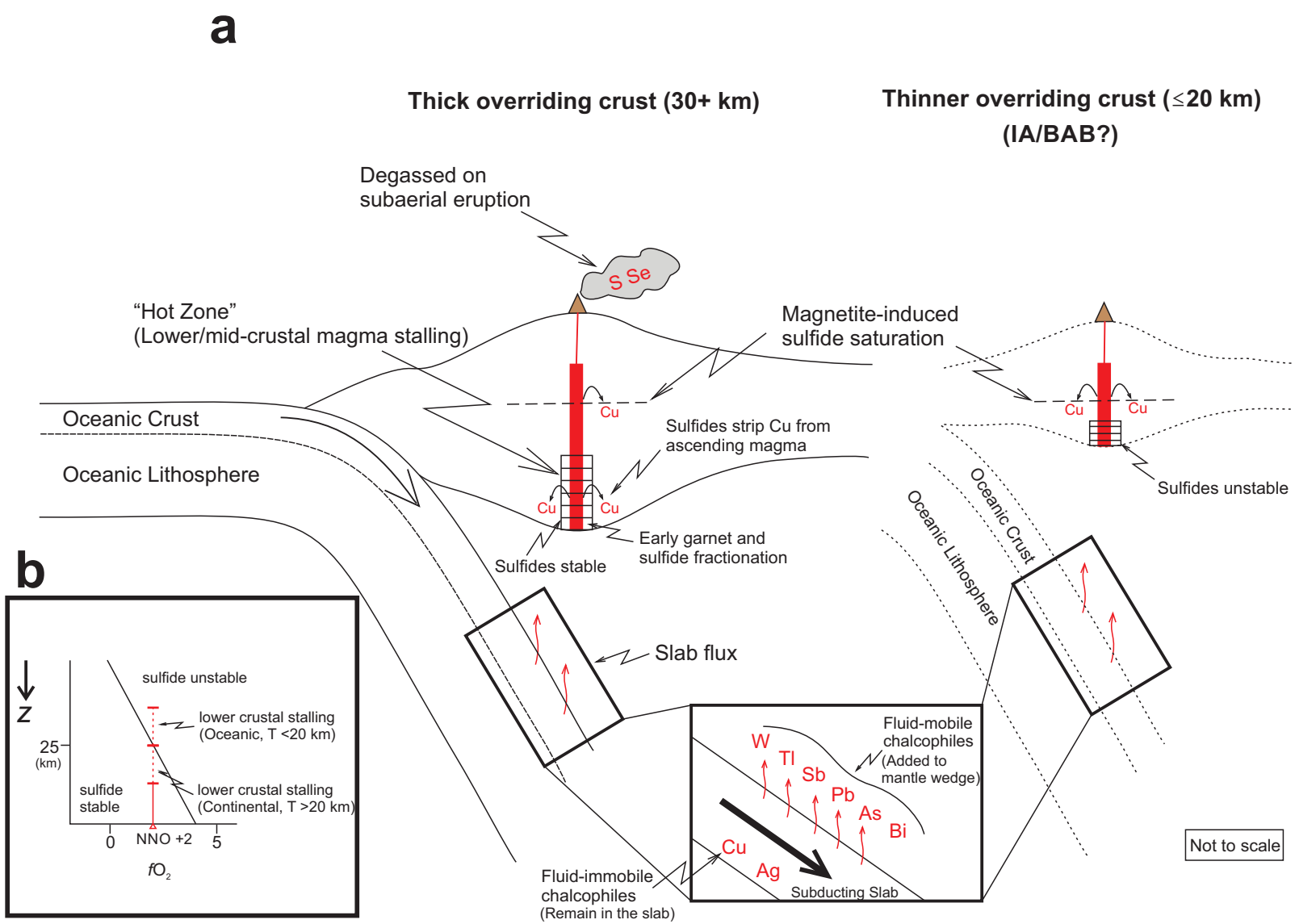

Figure

Click here to download Figure: Cox_et_al_Figure7.pdf

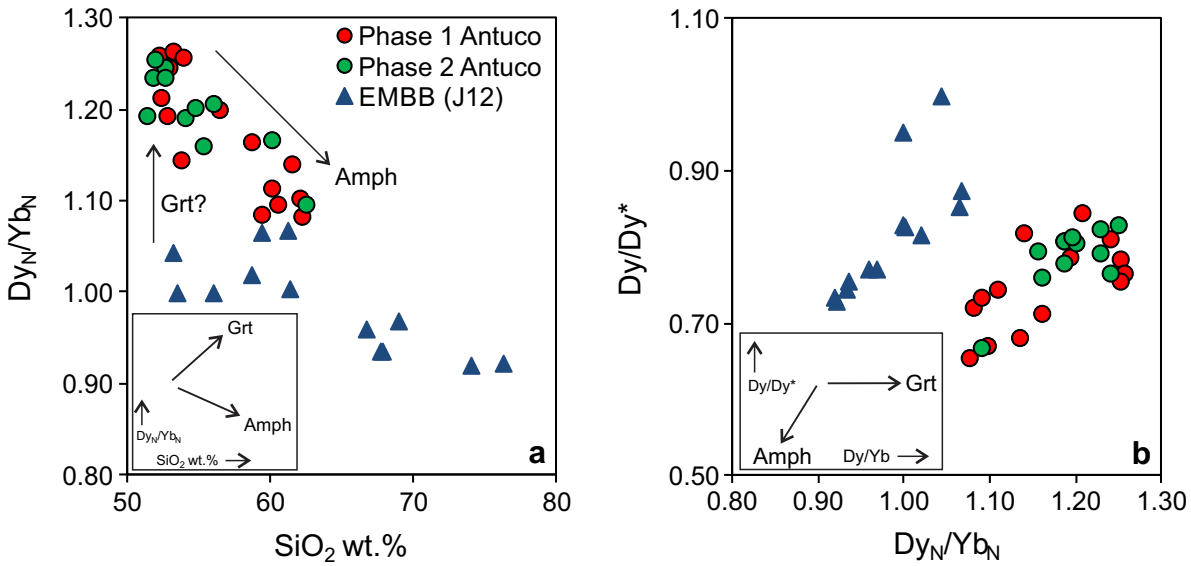

Figure

Click here to download Figure: Cox_et_al_Figure8.pdf

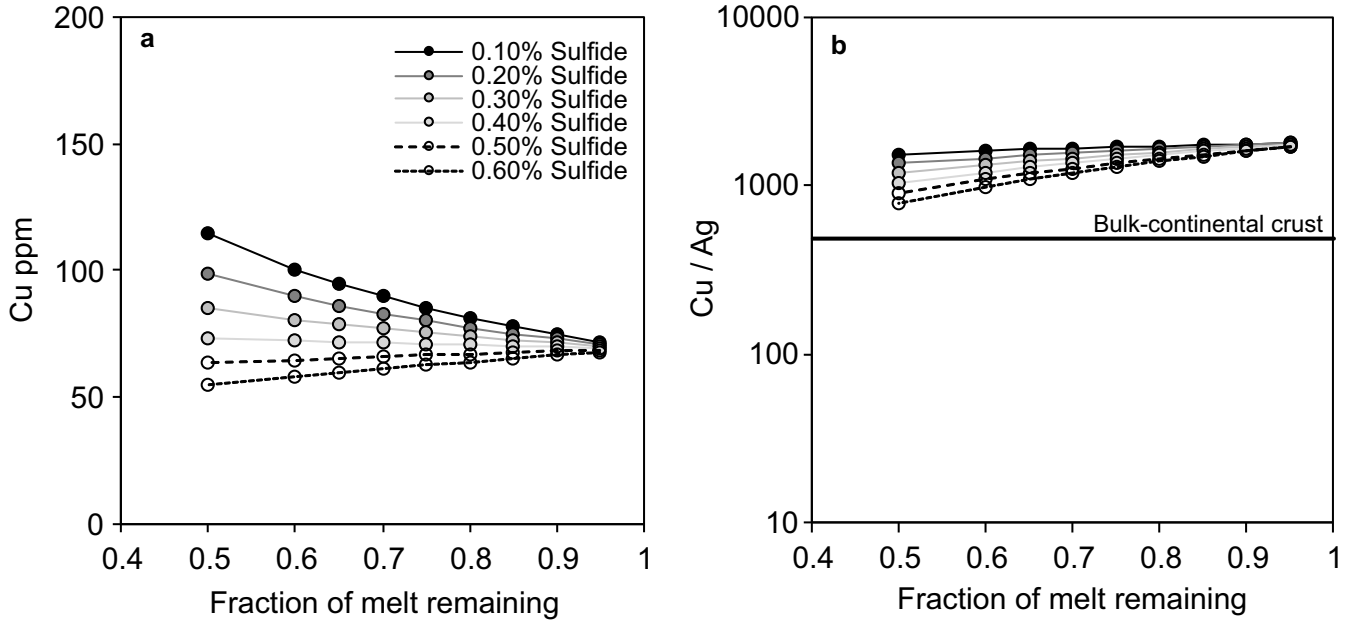

Table 1 Fractional crystallisation modelling parameters

	Plagioclase / Olivine	**Sulphide**
Mineral proportion	0.994	0.006
Kd	**Cu**	**Ag**
Plagioclase / Olivine	0.05	0.001
Sulphide (crystalline)	215	24
Do	1.340	0.145
Co (An27-7)	68.923	0.038

Kd: Partition coefficient for a particular element in a mineral, Do: Bulk-distribution coefficient of a particular element prior to fractional crystallisation, Co: Concentration of a particular element in the source.